DALTON
FULL PAPER

Synthesis, crystal structures, spectroscopic and electrochemical properties of homologous series of copper(II) complexes of Schiff bases derived from cycloalkylamines

Martha Aguilar-Martínez, Ricardo Saloma-Aguilar, Norma Macías-Ruvalcaba, Raúl Cetina-Rosado,† Agustina Navarrete-Vázquez, Virginia Gómez-Vidales, Arturo Zentella-Dehesa, Rubén A. Toscano, Simón Hernández-Ortega and Juan M. Fernández-G.*

Instituto de Química, U.N.A.M. Circuito Exterior, Ciudad, Universitaria Coyoacán 04510, México, D.F. México

Received 23rd October 2000, Accepted 17th May 2001
First published as an Advance Article on the web 31st July 2001

Six Schiff base copper(II) complexes have been prepared and characterized, elemental analyses, mass, IR and electronic spectra, μ_{eff} and X-ray crystal structures being obtained. The X-ray study shows that the geometry around the metal atom is square planar for one of the complexes only and distorted square planar for the others. Electrochemical studies on the complexes, though revealing a dependence of the Cu(II)/Cu(I) potentials on electronic effects, also show that these are independent of the structure observed in the solid state. Besides, EPR studies of these complexes in DMF solution at 193 K suggest that the geometry of these complexes in solution is different to that observed in the solid state by X-ray crystallography.

Introduction

There is a continuing interest in investigating the relationship between the redox potentials and other electrochemical parameters in solution with the geometry of bis-bidentate Schiff base metal complexes in the solid state,[1,2] which could be the result of steric effects,[3] electronic effects[4] or crystal packing forces.[5]

We have recently described the crystal structures and electrochemical studies of some copper(II) complexes of 2,3-naphthalenic Schiff bases derived from cycloalkylamines,[6] (Cu–2,3-*N*-cycloalkyl). These complexes have shown an interesting relationship between the grade of distortion observed in the solid state *vs.* the Cu(II)/Cu(I) cathodic peak potentials (E_{pc}); this relationship is inverse to the reported trend shown by the series of salicylaldamine copper(II) complexes, where an alkyl instead of a cycloalkyl substituent is present[1] and where it was found that nonplanar bis-chelate complexes are easier to reduce than their planar analogs, *i.e.* the less negative the E_{pc} the more voluminous the alkyl substituent.

In this paper, the synthesis, crystal structures, cyclic voltammetry and other electrochemical measurements for the analogous Schiff base copper(II) complexes derived from salicylaldehyde and 2-hydroxy-1-naphthaldehyde with the corresponding cycloalkylamines are described, *i.e.* bis-{(cyclopentyl)[(2-oxo-1*H*-benzo-1-ylidene)methyl]aminato}copper(II) (**1**), bis{(cycloheptyl)[(2-oxo-1*H*-benzo-1-ylidene)methyl]aminato}copper(II) (**2**), bis{(cyclooctyl)[(2-oxo-1*H*-benzo-1-ylidene)methyl]-aminato}copper(II) (**3**), bis{(cyclopentyl)[(2-oxo-1*H*-naphth-1-ylidene)methyl]aminato}copper(II) (**4**), bis{(cycloheptyl)[(2-oxo-1*H*-naphth-1-ylidene)methyl] aminato}copper(II) (**5**) and bis{(cyclooctyl)[(2-oxo-1*H*-naphth-1-ylidene)methyl]aminato}-copper(II) (**6**) in order to explore the dependence of the Cu(II)/Cu(I) potentials on the structure of the complexes and also to compare both sets of data **1**–**3** (Cu–sal-*N*-cycloalkyl) and **4**–**6** (Cu–1,2-*N*-cycloalkyl), where the cycloalkyl group contains 5, 6, 7 or 8 carbon atoms, with the corresponding information for similar Schiff base copper(II) complexes (Cu–2,3-*N*-cycloalkyl).[6] Finally, EPR measurements were performed so that they could be used as a means of tracing the extent of distortion from the planar structure for the solution phase of these series of complexes, including the homolog already described,[6] by using the coupling constant $A_{\parallel}$ as a measure of this distortion.

Results and discussion

All compounds are soluble in dichloromethane or chloroform but less soluble in solvents such as alcohols, tetrahydrofuran, benzene and ethyl acetate. The elemental analyses were satisfactory, indicating that the complexes have a ligand-to-metal ratio of 2 : 1. The mass spectra of the complexes indicate that the expected molecular ions display the characteristic copper isotopic distribution, which agrees with the 2 : 1 ligand-to-metal stoichiometric ratio. $[M^+ + H]$ ions were also detected, as is usual in FAB mass spectra.[7] The values of the magnetic moments for all the complexes are in the range of those described for planar to pseudo-tetrahedral n-alkyl-salicylideneaminato copper(II) complexes, *i.e.* 1.83–1.93 B.M.[8] The infrared spectra show the ν(C=N) vibration around 1612 cm^{-1}, which is characteristic in these systems.[9] The electronic spectra of complexes **1**–**3** show a band associated with $d \rightarrow d$ transitions around 660 nm with an ε around 155, all the other bands being attributable to charge transfer or intraligand transitions, although for the spectra of naphthalenic complexes **4**–**6** we were unable to obtain bands corresponding to transitions in the ligand field region, only intraligand or charge transfer bands were observed.[8]

Crystal data, and additional data collection parameters and refinement details are given in Table 1. Selected bond lengths and angles are given in Table 2. The molecular structure of compounds **1** and **5** including atom-numbering schemes are illustrated in Fig. 1 and 2. The X-ray diffraction analysis of **1**–**6** shows that the copper ion is bonded to the oxygen and nitrogen donor atoms of the two ligand molecules in the usual *trans* arrangement in which the copper ion is four coordinate. An interesting feature in the unit cell of compound **6**, is that there

† Deceased.

 DOI: 10.1039/b104892a

Table 1 Crystallographic data for compounds **1**–**6**

Compound	**1**	**2**	**3**	**4**	**5**	**6**
Chemical formula	$C_{24}H_{28}N_2O_2Cu$	$C_{28}H_{36}N_2O_2Cu$	$C_{30}H_{40}N_2O_2Cu$	$C_{32}H_{32}N_2O_2Cu$	$C_{36}H_{40}N_2O_2Cu$	$C_{76}H_{88}N_4O_4Cu_2$
Formula weight	440.02	496.13	524.18	540.14	596.24	1248.58
Crystal system	Monoclinic	Monoclinic	Monoclinic	Monoclinic	Monoclinic	Triclinic
Space group	$P2(1)/c$	$P2(1)/c$	$P2_1/c$	$P2_1/c$	$P2_1/c$	$P\bar{1}$
μ(Mo-Kα)mm^{-2}	1.019	0.912	0.813	0.871	0.793	0.719
T/K	293(2)	293(2)	293(2)	293(2)	293(2)	293(2)
Unit cell dimensions						
a/Å	12.306(1)	19.543(2)	12.937(2)	12.5316(2)	9.239(1)	13.731(3)
b/Å	16.143(2)	10.067(2)	17.112(2)	20.085(4)	9.140(1)	14.024(3)
c/Å	12.149(1)	12.624(2)	13.358(2)	10.531(2)	17.190(1)	17.181(3)
α/°	90	90	90	90	90	93.31
β/°	114.89(1)	96.53(2)	109.84(1)	91.17(2)	96.037(6)	101.10
γ/°	90	90	90	90	90	98.54
Unit cell volume/Å^3	2189.3(4)	2467.5(5)	2781.8(7)	2604.5(8)	1443.5(2)	3197.8(11)
Z	4	4	4	4	2	2
Measured/independent reflections	4789/3865	5320/4330	4846/4616	4856/4589	2707/2541	11829/11311
R_{int}	0.0378	0.0345	0.0346	0.0551	0.0381	0.0471
Final R indices [$I > 2\sigma(I)$]						
R_1	0.0571	0.0411	0.0693	0.0675	0.0432	0.0554
wR_2	0.1324	0.846	0.1714	0.1438	0.099	0.12

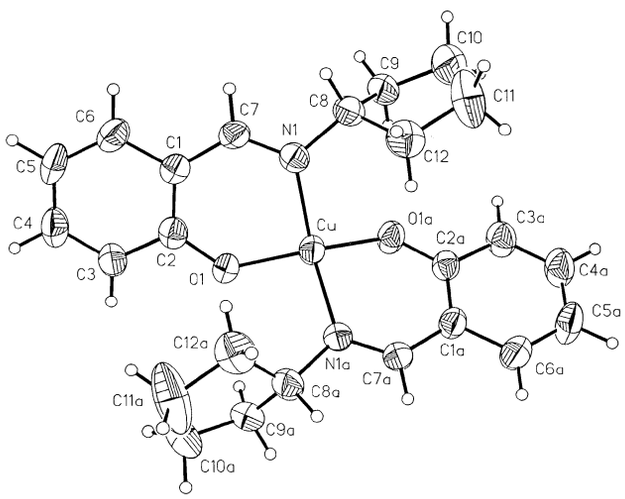

Fig. 1 Molecular structure of **1** in the solid state with atom numbering scheme. Thermal ellipsoids are drawn at 50% probability.

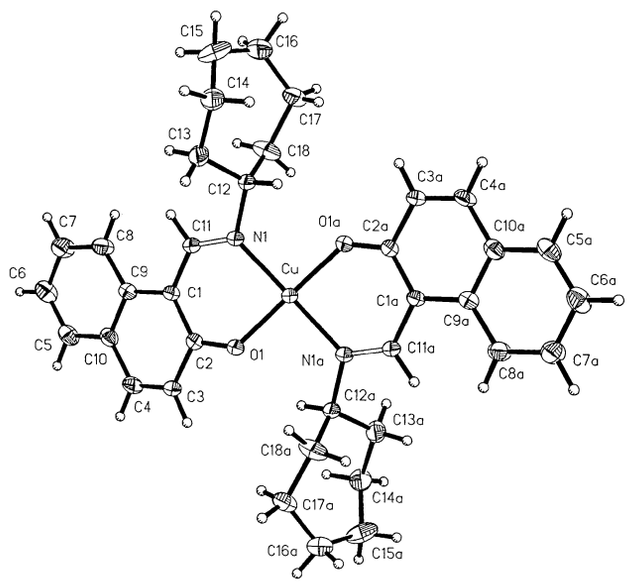

Fig. 2 Molecular structure of **5** in the solid state with atom numbering scheme. Thermal ellipsoids are drawn at 50% probability.

are two crystallographically independent but structurally very similar molecules, **6a** and **6b**, differing only in the dihedral angle between the two coordination planes defined by O(1)–Cu–N(1) and O(2)–Cu–N(2). While the geometry in **5** is stepped square planar (with a step of 1.22 Å), complexes **1**–**4**, **6a** and **6b** have very similar structures with geometries intermediate between square planar and tetrahedral, where the dihedral angles between the two coordination planes defined by O(1)–Cu–N(1) and O(2)–Cu–N(2) are 54.9, 25.2, 46.3, 42.0, 40.6 and 48.1°, respectively. Bond angles in **1**–**4**, **6a** and **6b**, also show that the coordination geometry about the copper atom is distorted square planar, with N(1)–Cu–N(2) ranging from 140.9(2) to 162.94(11)° and O(1)–Cu–O(2) angles from 140.0(2) to 160.94(11)°. Other angles show expected values.

The Cu–O and Cu–N bonds in **1**–**6** have similar lengths and are in the same range as those reported for similar copper(II) complexes,[6b] *i.e.* Cu–O distances are in the range 1.868(4)–1.901(4) Å, while Cu–N distances are between 1.962(4) and 2.019(3) Å. However, Cu–N bond lengths in all these complexes are slightly shorter than those reported for a similar salicylideneaminato copper(II) complex where a cyclohexyl substituent is attached to the imine nitrogen,[10] which shows Cu–N bond lengths of 2.034(2) Å. Despite the fact that a cyclopentyl group is less bulky than *tert*-butyl, complex **1** is as distorted (dihedral angle 54.9°) as the analogous bis[*N*-(*tert*-butyl)salicylideneaminato]copper(II)[11] complex, which shows a dihedral angle of 54°.

Table 3 shows the electrochemical data obtained at a Pt electrode in deoxygenated DMF solution, with Et_4NBF_4 as supporting electrolyte, of 1 mM of the Cu(II) complexes at sweep rates of 25 to 1000 mV s^{-1} for cyclic voltammetry and 10–100 ms width pulses for chronocoulometric studies. The cyclic voltammograms recorded in the potential range 0.0 to −2.0 V *vs.* SCE show for all the copper(II) complexes a similar electrochemical behaviour. The one-electron reduction peak (E_{pc}), corresponding to the $Cu^{II}L_2/[Cu^{I}L_2]^-$ reaction, occurs in the potential range −735 to −950 mV, with a directly associated reoxidation peak (E_{pa}) in the reverse scan, whose potential values fall within the range −620 to −686 mV (Table 3). In Fig. 3, this general electrochemical response is illustrated by the voltammogram of compound **4**. Analysis of the cyclic voltammetric responses to scan rates showed the following features: the anodic to cathodic peak current ratio (I_{pa}/I_{pc}) decreased at faster scan rates, as is shown in Fig. 4 for complex **4**; the difference between the potential of the anodic peak and that of the cathodic peak ($E_{pa} - E_{pc} = \Delta E_p$) gradually increased from 113 to 940 mV, going from 25 to 1000 mV s^{-1}, thus indicating that the system deviates strongly from reversibility at high sweep rates. These data are diagnostic for a simple quasi-reversible one-electron charge transfer.[12] Furthermore, the plot shows a

Table 2 Selected bond lengths (Å) and angles (°) for compounds **1**–**6**

Compound **1**			
Cu–O(1)	1.887(4)	O(1)–Cu–O(1a)	140.0(2)
Cu–O(1a)	1.889(4)	O(1)–Cu–N(1a)	99.2(2)
Cu–N(1)	1.998(5)	O(1)–Cu–N(1)	94.3(2)
Cu–N(1a)	1.991(5)	O(1a)–Cu–N(1)	98.5(2)
O(1)–C(2)	1.308(6)	O(1a)–Cu–N(1a)	94.2(2)
N(1)–C(7)	1.282(7)	N(1)–Cu–N(1a)	140.9(2)
N(1)–C(8)	1.478(7)	C(2)–O(1)–Cu	127.8(4)
C(1)–C(7)	1.437(8)	C(7)–N(1)–Cu	121.9(4)
C(1)–C(2)	1.416(8)	C(8)–N(1)–Cu	121.2(4)
C(2)–C(3)	1.410(8)	O(1)–C(2)–C(1)	123.7(5)
C(3)–C(4)	1.369(9)	N(1)–C(7)–C(1)	128.0(5)
Compound **2**			
Cu–O(1)	1.887(2)	O(1)–Cu–O(1a)	160.94(11)
Cu–O(1a)	1.889(2)	O(1)–Cu–N(1a)	90.48(10)
Cu–N(1)	2.004(3)	O(1)–Cu–N(1)	92.49(11)
Cu–N(1a)	2.019(3)	O(1a)–Cu–N(1)	91.11(11)
O(1)–C(2)	1.304(4)	O(1a)–Cu–N(1a)	91.54(11)
N(1)–C(7)	1.280(4)	N(1)–Cu–N(1a)	162.94(11)
N(1)–C(8)	1.495(4)	C(2)–O(1)–Cu	129.6(2)
C(1)–C(7)	1.439(5)	C(7)–N(1)–Cu	123.6(2)
C(1)–C(2)	1.411(5)	C(8)–N(1)–Cu	119.0(2)
C(2)–C(3)	1.420(5)	O(1)–C(2)–C(1)	124.3(3)
C(3)–C(4)	1.364(5)	N(1)–C(7)–C(1)	127.8(3)
Compound **3**			
Cu–O(1)	1.878(5)	O(1)–Cu–O(1a)	146.1(2)
Cu–O(1a)	1.891(5)	O(1)–Cu–N(1a)	94.6(2)
Cu–N(1)	1.980(6)	O(1)–Cu–N(1)	94.5(2)
Cu–N(1a)	1.973(6)	O(1a)–Cu–N(1)	96.3(2)
O(1)–C(2)	1.306(8)	O(1a)–Cu–N(1a)	93.7(2)
N(1)–C(7)	1.300(8)	N(1)–Cu–N(1a)	146.9(2)
N(1)–C(8)	1.486(9)	C(2)–O(1)–Cu	128.2(5)
C(1)–C(7)	1.420(10)	C(7)–N(1)–Cu	121.8(5)
C(1)–C(2)	1.411(10)	C(8)–N(1)–Cu	120.8(5)
C(2)–C(3)	1.394(9)	O(1)–C(2)–C(1)	124.4(6)
C(3)–C(4)	1.360(11)	N(1)–C(7)–C(1)	128.6(7)
Compound **4**			
Cu–O(1)	1.878(4)	O(1)–Cu–O(1a)	149.2(2)
Cu–O(1a)	1.895(4)	O(1)–Cu–N(1)	92.1(2)
Cu–N(1)	1.993(6)	O(1a)–Cu–N(1a)	92.7(2)
Cu–N(1a)	1.989(5)	O(1a)–Cu–N(1)	94.8(2)
O(1)–C(2)	1.310(8)	O(1)–Cu–N(1a)	95.8(2)
N(1)–C(11)	1.294(8)	N(1)–Cu–N(1a)	150.8(2)
N(1)–C(12)	1.478(8)	C(2)–O(1)–Cu	127.3(4)
C(1)–C(11)	1.428(9)	C(11)–N(1)–Cu	122.0(5)
C(1)–C(2)	1.411(9)	C(12)–N(1)–Cu	120.3(4)
C(2)–C(3)	1.430(9)	N(1)–C(11)–C(1)	128.5(6)
C(3)–C(4)	1.335(10)	O(1)–C(2)–C(1)	124.5(6)
Compound **5**			
Cu–O(1)	1.898(2)	O(1)–Cu–O(1a)	180.0
Cu–O(1a)	1.898(2)	O(1)–Cu–N(1)	89.68(9)
Cu–N(1)	2.000(2)	O(1a)–Cu–N(1a)	89.68(9)
Cu–N(1a)	2.000(2)	O(1a)–Cu–N(1)	90.32(9)
O(1)–C(2)	1.301(4)	O(1)–Cu–N(1a)	90.32(9)
N(1)–C(11)	1.286(4)	N(1)–Cu–N(1a)	180.0
N(1)–C(12)	1.493(3)	C(2)–O(1)–Cu	127.8(2)
C(1)–C(11)	1.445(4)	C(11)–N(1)–Cu	123.49(19)
C(1)–C(2)	1.405(4)	C(12)–N(1)–Cu	119.98(19)
C(2)–C(3)	1.437(4)	N(1)–C(11)–C(1)	127.7(3)
C(3)–C(4)	1.343(6)	O(1)–C(2)–C(1)	124.3(3)
Compound **6**			
Cu(1)–O(1)	1.868(4)	O(1)–Cu(1)–O(2)	146.14(18)
Cu(1)–O(2)	1.891(4)	O(1)–Cu(1)–N(1)	92.94(16)
Cu(1)–N(1)	1.970(4)	O(2)–Cu(1)–N(2)	93.13(16)
Cu(1)–N(2)	1.967(4)	O(2)–Cu(1)–N(1)	98.05(16)
O(1)–C(2)	1.310(6)	O(1)–Cu(1)–N(2)	95.97(16)
N(1)–C(11)	1.289(6)	N(1)–Cu(1)–N(2)	145.02(17)
N(1)–C(12)	1.495(6)	C(2)–O(1)–Cu(1)	130.2(3)
C(1)–C(11)	1.448(7)	C(11)–N(1)–Cu(1)	123.6(4)
C(1)–C(2)	1.407(7)	C(12)–N(1)–Cu(1)	120.2(3)
C(2)–C(3)	1.424(7)	N(1)–C(11)–C(1)	127.8(5)
C(3)–C(4)	1.347(8)	O(1)–C(2)–C(1)	123.7(5)
Cu(2)–O(1a)	1.901(4)	O(1a)–Cu(2)–O(2a)	150.35(18)
Cu(2)–O(2a)	1.890(4)	O(1a)–Cu(2)–N(1a)	92.10(16)
Cu(2)–N(1a)	1.981(4)	O(2a)–Cu(2)–N(2a)	92.43(16)
Cu(2)–N(2a)	1.962(4)	O(2a)–Cu(2)–N(1a)	94.93(17)
O(1a)–C(2a)	1.300(6)	O(1a)–Cu(2)–N(2a)	94.15(16)
N(1a)–C(11a)	1.291(6)	N(1a)–Cu(2)–N(2a)	153.18(18)
N(1a)–C(12a)	1.486(6)	C(2a)–O(1a)–Cu(2)	128.1(3)
C(1a)–C(11a)	1.420(7)	C(11a)–N(1a)–Cu(2)	122.8(4)
C(1a)–C(2a)	1.402(7)	C(12a)–N(1a)–Cu(2)	119.9(3)
C(2a)–C(3a)	1.437(7)	N(1a)–C(11a)–C(1a)	128.9(5)
C(3a)–C(4a)	1.336(7)	O(1a)–C(2a)–C(1a)	124.4(5)

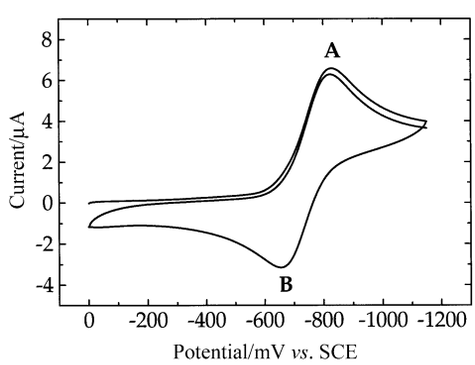

Fig. 3 Cyclic voltammogram recorded at a Pt electrode (3.14 mm²) in a DMF solution containing complex **4** (0.6×10^{-3} mol dm^{-3}) and Et_4NBF_4 (0.1 mol dm^{-3}), scan rate 100 mV s^{-1}.

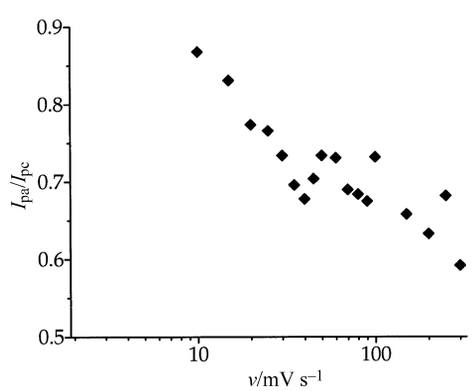

Fig. 4 Plot of the ratio of anodic to cathodic peak currents (I_{pa}/I_{pc}) as a function of scan rate (v) for compound **4**.

linear relationship that does not intercept at the origin between cathodic current (I_{pc}) and the square root of the sweep rate ($v^{1/2}$) for **4** (Fig. 5). This behaviour is characteristic of the presence of kinetic complications.[12] It is well known that the $Cu^{II}L_2$/$[Cu^{I}L_2]^-$ reaction in most CuN_2O_2 coordination complexes is quasi-reversible in nature due to the fact that the $[Cu^{I}L_2]^-$ species are chemically decomposed to a copper ion (reaction 1, pathway a), which subsequently is reduced to copper metal[1] (reaction (1), pathway b).

$$[Cu^{I}L_2]^- \underset{a}{\overset{k}{\rightleftharpoons}} Cu^+ + 2L^- \underset{b}{\overset{e}{\rightleftharpoons}} Cu^0 + 2L^- \qquad (1)$$

Table 3 Kinetic[a] and electrochemical[b] parameters for the reduction process of Cu–sal-*N*-cycloalkyl **1**–**3**, Cu–1,2-*N*-cycloalkyl **4**–**6**, and Cu–2,3-*N*-cycloalkyl[c] in DMF solution, compared with the dihedral angle between the two coordination planes defined by O(1)–Cu–N(1) and O(2)–Cu–N(2) observed in the solid state for the corresponding complexes

Compound		E_{pc}/mV	E_{pa}/mV	ΔE_p/mV	I_{pa}/I_{pc}	$k_s/10^{-4}$ cm s^{-1}	$k/10^{-5}$ s^{-1}	E_s[d]	Dihedral angle/°
Cu–sal-*N*-cypen	**1**	−827	−641	186	0.68	17.57	2.24	0.41	54.9
Cu–sal-*N*-cyhex[e]	—	−869	−686	183	0.47	3.52	5.39	0.69	0
Cu–sal-cyhep	**2**	−916	−660	256	0.56	[f]	6.00	0.92	25.2
Cu–sal-*N*-cyoct	**3**	−917	−644	273	0.39	[f]	6.21	[g]	46.3
Cu–1,2-*N*-cypen	**4**	−850	−635	215	0.71	12.50	2.47	0.41	42.0
Cu–1,2-*N*-cyhex[e]	—	−904	−620	284	0.58	7.54	5.78	0.69	0
Cu–1,2-*N*-cyhep	**5**	−930	−639	291	0.35	2.29	11.44	0.92	0
Cu–1,2-*N*-cyoct	**6**	−950	−639	311	0.16	1.04	[f]	[g]	40.6; 48.1
Cu–2,3-*N*-cypen[c]	—	−735	−632	103	0.81	14.27	1.12	0.41	32.9
Cu–2,3-*N*-cyhex[e]	—	−774	−651	123	0.61	4.58	3.03	0.69	39
Cu–2,3-*N*-cyhep[c]	—	−798	−651	147	0.58	7.45	3.23	0.92	43
Cu–2,3-*N*-cyoct[c]	—	−862	−629	233	0.48	3.72	4.03	[g]	53

[a] Measured by double potential step chronocoulometry. [b] Measured by cyclic voltammetry *vs.* SCE. [c] From ref. 6*a*. [d] From ref. 14. [e] From ref. 6*b*. [f] Data not available due to system irreversibility. [g] Data not reported in the literature.

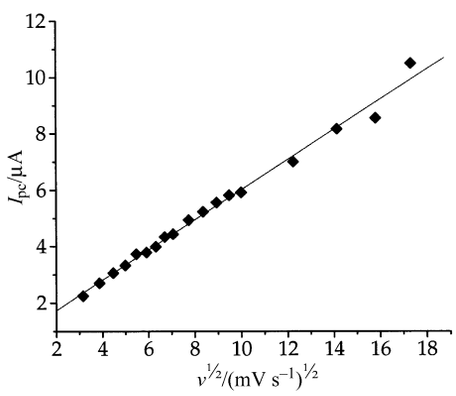

Fig. 5 Cathodic current (I_{pc}) *versus* square root of sweep rate ($v^{1/2}$) for compound **4**.

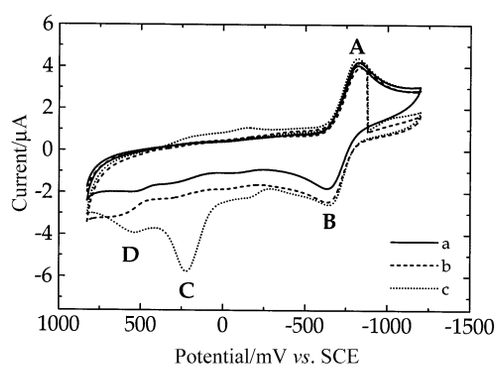

Fig. 6 Cyclic voltammograms recorded at (a) a platinum electrode (3.14 mm^2) in a DMF solution containing complex **4** (1×10^{-3} mol dm^{-3}) and Et_4NBF_4 (0.1 mol dm^{-3}), scan rate 100 mV s^{-1}; and after controlled potential at −887 mV for (b) 1 min; and (c) for 2 min.

In order to determine that the $[Cu^IL_2]^-$ species decomposes following pathway a, microelectrolysis experiments for complexes **1**–**6** were carried out for one and two min. at their respective E_{pc} reduction potentials of peak A, as exemplified by **4** in Fig. 6. In all cases the corresponding anodic wave (peak B) was observed, indicating that species $[Cu^IL_2]^-$ are relatively stable under these conditions; however, part of it decomposes according to the above mentioned pathways a and b, as observed by the presence of two anodic peaks C and D assigned to the pathways c and d respectively in reaction 2:

$$Cu^0 \underset{c}{\overset{-e}{\rightleftharpoons}} Cu^+ \underset{d}{\overset{-e}{\rightleftharpoons}} Cu^{2+} \qquad (2)$$

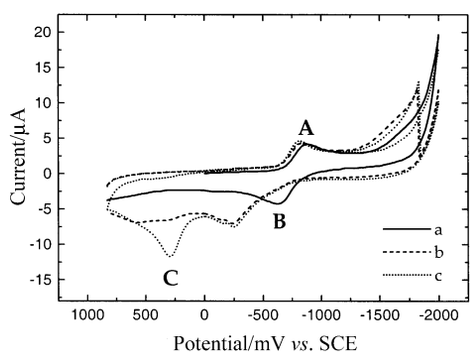

Fig. 7 Cyclic voltammograms recorded at (a) a platinum electrode (3.14 mm^2) in a DMF solution containing complex **4** (1×10^{-3} mol dm^{-3}) and Et_4NBF_4 (0.1 mol dm^{-3}), scan rate 100 mV s^{-1}; and after controlled potential at −1841 mV for (b) 1 min; and (c) 2 min.

The homogeneous chemical rate constant (k) for the reaction corresponding to pathway a, was obtained from chronocoulometry experiments (Table 3). This constant has a value of 2.47×10^{-5} s^{-1} for **4**, which, as for the other complexes, lies between 0 and 10^3 s^{-1}, characteristic of a slow chemical reaction.[13]

The heterogeneous electrochemical rate constant (k_s) for the system $Cu^{II}L_2/[Cu^IL_2]^-$ was obtained by cyclic voltammetry for all the complexes of these three series (Table 3). The k_s values were found to be in the range of quasi-reversible systems $10^{-1} > k_s > 10^{-5}$ cm s^{-1}, thus indicating slow electron transfer kinetics, which is due to the stereochemical changes that accompany the $Cu^{II}L_2/[Cu^IL_2]^-$ redox step, rather than to an intrinsic aspect of the heterogeneous charge transfer.[14]

Near the cathodic window of the Et_4NBF_4/DMF system (−2000 mV) all complexes exhibit a second cathodic step which is attributable to the $[Cu^IL_2]^-/[Cu^0L_2]^{2-}$ redox change, lacking a directly associated response in the reverse scan because of the rapid demetallation of the $[Cu^0L_2]^{2-}$ species (reaction 3,

$$[Cu^0L_2]^{2-} \underset{e}{\overset{k}{\rightleftharpoons}} Cu^0 + 2L^- \qquad (3)$$

pathway e). This was confirmed when the microelectrolyses for 1 and 2 min. at a potential near the cathodic window were carried out, where peak C in the cyclic voltammogram of **4** (Fig. 7) is associated with the reoxidation of electrodeposited copper metal to free Cu^+. In addition, an irreversible anodic process due to ligand oxidation is present at about 1000 mV for all complexes (data not shown).

As far as the above results are concerned, complexes **1**–**6** and those of the Cu–2,3-*N*-cycloalkyl series show similar

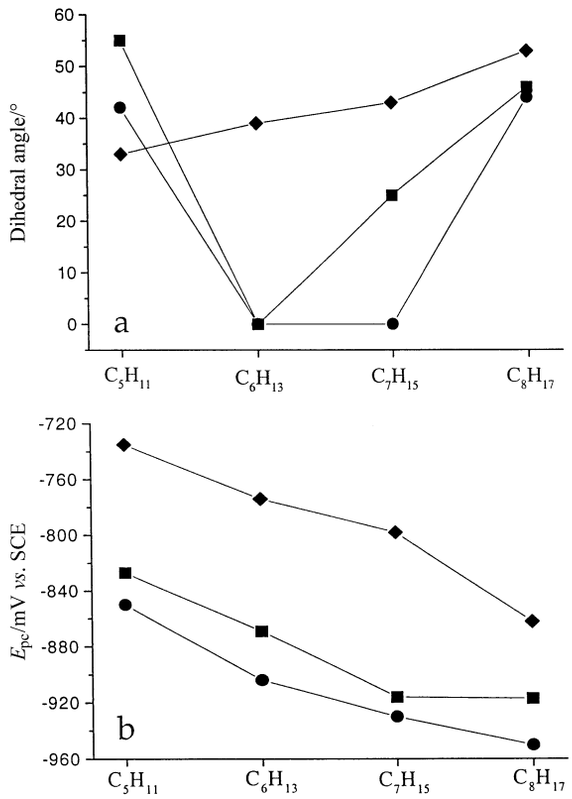

Fig. 8 (a) Dihedral angle values as a function of the cycloalkyl substituent size at the coordinating nitrogen atom for the Schiff base Cu(II) complexes **1**–**6**. Cu–sal-*N*-cycloalkyl series (■), Cu–1,2,-*N*-cycloalkyl series (●) and Cu–2,3-*N*-cycloalkyl series (◆) (from ref. 6). (b) Reduction potentials (E_{pc}) as a function of the cycloalkyl substituent size at the coordinating nitrogen atom for the Schiff base Cu(II) complexes **1**–**6**. Cu–sal-*N*-cycloalkyl (■), Cu–1,2-*N*-cycloalkyl (●) and Cu–2,3-*N*-cycloalkyl (◆) (from ref. 6).

electrochemical behavior (Table 3), and the following observations emerge. (i) The E_{pc} values for each series, change gradually toward a more negative potential as the cycloalkyl substituent becomes more voluminous. Thus, the reduction potentials E_{pc} decrease as follows: $C_5H_9 > C_6H_{11} > C_7H_{13} > C_8H_{15}$ (Fig. 8b) which indicates that for the complexes it is more difficult to approach the electrode as the substituent becomes bulkier. In fact, a linear relationship exists between the Taft steric constant (E_s)[15] and the E_{pc} values (Table 3). These results of cycloalkyl substituents are in contrast with those presented by Patterson and Holm,[1] who studied copper(II) chelates with alkyl substituents, where the E_{pc} reduction potentials were less negative as the alkyl substituent became more voluminous. They explained this as the result of favorable stereochemical assemblies in which, when the alkyl substituent is of lesser steric bulk (Me, Ph, n-Bu), the coordination around the metal ion is substantially square planar, while when the bulkiness of the substituents increases (*i*-Pr, *t*-Bu), significant tetrahedral distortions are present. With respect to the series studied in this research, it seems that the stability of the $[Cu^{I}L_2]^-$ species decreases when a bulkier substituent is present, causing the reduction process to become more difficult, this probably being accompanied by strong structural changes. In a previous paper,[6a] it was found that in the solid state the Cu–2,3-*N*-cycloalkyl series followed a trend in which, as the size of the cycloalkyl increased, the extent of distortion also increased and the E_{pc} values became more cathodic. However, in the corresponding Cu–sal-*N*-cycloalkyl and Cu–1,2-*N*-cycloalkyl series, the relationship between E_{pc} values and the extent of distortion in the solid state is not so straightforward. (ii) In the three series, E_{pc} reduction potentials diminish in the order Cu–1,2-*N*-cycloalkyl < Cu–sal-*N*-cycloalkyl < Cu–2,3-*N*-cycloalkyl. It is important to point out that these results are a consequence of

Table 4 Coupling constant $A_{\parallel}$ (±0.1 mT), $g_{\parallel}$ and $g_{\perp}$ values for the series Cu–sal-*N*-cycloalkyl, Cu–1,2-*N*-cycloalkyl and Cu–2,3-*N*-cycloalkyl in DMF solution

Compound		$g_{\parallel}$	$g_{\perp}$	$A_{\parallel}$/mT
Cu–sal-*N*-cypen	**1**	2.2312	2.0551	15.39
Cu–sal-*N*-cyhex[a]	—	2.2287	2.0545	16.89
Cu–sal-cyhep	**2**	2.2382	2.0555	15.62
Cu–sal-*N*-cyoct	**3**	2.2317	2.0541	16.63
Cu–1,2-*N*-cypen	**4**	2.1551	2.0691	—
Cu–1,2-*N*-cyhex[a]	—	2.2410	2.0573	16.36
Cu–1,2-*N*-cyhep	**5**	2.2316	2.0546	15.86
Cu–1,2-*N*-cyoct	**6**	2.2355	2.0547	16.13
Cu–2,3-*N*-cypen[b]	—	2.2383	2.0536	15.65
Cu–2,3-*N*-cyhex[a]	—	2.2384	2.0597	16.13
Cu–2,3-*N*-cyhep[b]	—	2.2332	2.0537	16.33
Cu–2,3-*N*-cyoct[b]	—	2.2381	2.0504	16.46

[a] From ref. 6*b*. [b] From ref. 6*a*.

an electronic effect. The magnitude of the charge density at the C(1)–C(2) bonds in the aromatic rings of Cu–1,2-*N*-cycloalkyl and Cu–sal-*N*-cycloalkyl are comparable and able to exert a strong electronic effect toward the metal centre.[16] For this reason, the E_{pc} values for both the Cu–1,2-*N*-cycloalkyl and Cu–sal-*N*-cycloalkyl series of complexes are closer (Fig. 8), *i.e.* the E_{pc} values for Cu–sal-*N*-cycloalkyl are around 30 mV less negative than those for Cu–1,2-*N*-cycloalkyl, where stronger ligand fields probably exist. The Cu–2,3-*N*-cycloalkyl series, having a lower charge density at the C(2)–C(3) positions, have E_{pc} values of around 100 mV, which are less negative than those of the Cu–1,2-*N*-cycloalkyl complexes. (iii) A departure from the electrochemical reversibility, and hence the high molecular reorganization involved in the one-electron reduction $Cu^{II}L_2/[Cu^{I}L_2]^-$ in these complexes, is evident from the large separation between peaks A and B ($\Delta E_p = E_{pa} - E_{pc}$) which are generally larger (103–311 mV) than expected for reversible systems (60 mV); moreover, the current relationship (I_{pa}/I_{pc}) was less than unity (0.16–0.71) in each case (Table 3). In these three series, it was observed that while the ΔE_p and the homogeneous chemical rate constant (k) increase, the relationship I_{pa}/I_{pc} and the heterogeneous electrochemical rate constant (k_s) become smaller as the size of the cycloalkyl ring substituent increased. The data agree with the fact that the bulk of the substituent is directly involved with the facility of the electron charge transfer and with the stability of the $[Cu^{I}L_2]^-$ species, which give rise to a chemical reaction coupled to the heterogeneous electron transfer $Cu^{II}L_2/[Cu^{I}L_2]^-$. It is worth noticing that the reversibility of these systems decreases in the order Cu–2,3-*N*-cycloalkyl > Cu–sal-*N*-cycloalkyl > Cu–1,2-*N*-cycloalkyl (Table 3).

A possible explanation for the observed E_{pc} trend in the Cu–sal-*N*-cycloalkyl and Cu–1,2-*N*-cycloalkyl series could be that in DMF solution, the complexes change the extent of their distortion observed in solid state in such a way that they follow the correlation observed by Holm and Patterson,[1] *i.e.* the less distorted complex shows the more negative E_{pc} value. Therefore, in order to obtain an adequate comparison of the electrochemical behavior of **1**–**6** with some other spectroscopic method, which could provide us with information in the solution phase about the extent of distortion from planarity of these complexes, several sets of EPR measurements in DMF solution were performed for all the Cu–sal-*N*-cycloalkyl, Cu–1,2-*N*-cycloalkyl and Cu–2,3-*N*-cycloalkyl[6] complexes, where, for all these series of complexes, the magnitude of the coupling constant $A_{\parallel}$ is taken as a measure of this distortion, in the sense that $A_{\parallel}$ values diminish as the geometry departs from axial configuration, *i.e.* the distortion grows.[17]

Except for complex **4**, where $A_{\parallel}$ can not be read off, the spectra allow the measurement of $g_{\parallel}$, $g_{\perp}$ and $A_{\parallel}$, the values of

which are shown in Table 4. In all cases, the samples show axial symmetry for the paramagnetic copper center.

Comparing voltammetric data (E_{pc}) with those from EPR ($A_{\|}$), it is noticeable that in all three series, as the size of the cycloalkyl group increases, the E_{pc} values become more negative. Furthermore by inspection of the corresponding $A_{\|}$ values, it is evident that for the Cu–1,2-*N*-cycloalkyl series, no clear correlation is observed, for the series Cu–sal-*N*-cycloalkyl there is no exact match but there appears to be a resemblance, while for the Cu–2,3-*N*-cycloalkyl series both trends match well. As the size of the cycloalkyl increases the $A_{\|}$ values increase as well, which could be interpreted as due to decreasing distortion.

If we now focus on the comparison between the EPR and crystallographic data, we can see for the Cu–2,3-*N*-cycloalkyl series that as the size of the cycloalkyl increases, the magnitude of the crystallographic dihedral angle grows but the $A_{\|}$ values increase as well (though they should diminish as distortion increases). Again, both trends in the other two series Cu–sal-*N*-cycloalkyl and Cu–1,2-*N*-cycloalkyl do not match. The main difference seems to be the X-ray crystallographic structures were determined from the solid phase, while EPR and voltammetric measurements were obtained from solutions, though at different temperatures. These differences could account for the observed behavior deviations.

Concluding remarks

The electrochemical properties of the complexes studied here are highly sensitive to the bulk of the cycloalkyl group and the electron density at the ligand. It is important to point out that the geometry or extent of distortion in the solid state of Schiff base copper(II) complexes of this kind has been usually interpreted as mainly dependent on steric considerations and sometimes complemented by electronic effects. However, in the solid state, the steric model applies only for the Cu–2,3-*N*-cycloalkyl series and the differences in the observed extent of distortion for the complexes of the Cu–sal-*N*-cycloalkyl and Cu–1,2-*N*-cycloalkyl series can be attributed mainly to crystal packing forces (Fig. 8a) which, due to their importance, are now currently acknowledged with the new insights into molecular recognition, self-organisation and supramolecular structures.[18] Nevertheless, in DMF solution, all three -*N*-cycloalkyl series of copper(II) Schiff bases change the geometry observed in the solid state.

Experimental

Reagents

Cyclopentylamine, cycloheptylamine, cyclooctylamine, copper(II) acetate monohydrate, salicylaldehyde, 2-hydroxy-1-naphthalenecarboxaldehyde and *N*,*N*-dimethylformamide (DMF) spectroscopic grade were obtained from Aldrich Chemical Co. Inc., and were used without further purification. Tetraethylammonium tetrafluoroborate (Et_4NBF_4) came from Fluka and was recrystallized from hexane–acetone and dried under vacuum at 60 °C for 8 h before use. Nitrogen was from Praxair and of ultra purity quality.

Physical measurements

The melting points were determined on a Fisher-Johns melting point apparatus and are uncorrected. Infrared spectra (KBr disks) were recorded on a Perkin-Elmer 203-B spectrophotometer and UV-visible spectra on a Shimadzu UV-160U recording spectrophotometer. Positive ion fast atom bombardment mass spectra were obtained on a JEOL JMS-SX-102A mass spectrometer operated at an accelerating voltage of 10 kV. Samples were desorbed from a nitrobenzyl alcohol matrix by using xenon atoms at 6 keV. Magnetic moment measurements were taken with a Johnson Matthey magnetic susceptibility balance at 24 °C. Elemental analyses were performed by Galbraith Laboratories, Inc. Knoxville, TN 37921–1750, USA.

Syntheses

The copper complexes **1**–**6** were prepared by methods described elsewhere.[19] The following preparation is a typical example of the general method.

To a solution of 0.002 mol (0.344 g) of 2-hydroxy-1-naphthalenecarboxaldehyde in 150 cm^3 of EtOH was added a solution of 0.002 mol of cyclopentylamine (0.162 g) in 60 cm^3 of EtOH followed by the addition of 0.0011 mol (0.220 g) of $Cu(OAc)_2 \cdot H_2O$ in 5 cm^3 of H_2O. The mixture was boiled under reflux for *ca.* 24 h, then concentrated until a precipitate was observed; the brown solid was filtered off under suction, washed with cold water and dried. Recrystallization from dichloromethane–methanol gave 0.43 g of complex **4** as deep brown–red crystals.

Bis{(cyclopentyl)[(2-oxo-1*H*-benzo-1-ylidene)methyl]-aminato}copper(II) 1. Yield 0.33 g, 75%; brown crystals; m.p. 110 °C. Found C, 65.6; H, 6.4; N, 6.5; calc. for $C_{24}H_{28}N_2O_2Cu$: C, 65.5; H, 6.4; N, 6.3%. FAB-MS *m*/*z*: M^+ 440 (base peak). IR (KBr): ν (C=N) 1613 cm^{-1}. μ_{eff} 1.90 B.M. UV/vis ($CHCl_3$) λ/nm (ε/M^{-1} cm^{-1}): 249 (34 270), 313 (9 000), 369 (10 930), 641 (157).

Bis{(cycloheptyl)[(2-oxo-1*H*-benzo-1-ylidene)methyl]-aminato}copper(II) 2. Yield 0.42 g, 85%; brown crystals; m.p. 173 °C. Found C, 67.8; H, 7.3; N, 5.7; calc. for $C_{28}H_{36}N_2O_2Cu$: C, 67.8; H, 7.3; N, 5.6%. FAB-MS *m*/*z*: M^+ 496 (base peak). IR (KBr): ν (C=N) 1614 cm^{-1}. μ_{eff} 1.90 B.M. UV/vis ($CHCl_3$) λ/nm (ε/M^{-1} cm^{-1}): 246 (41 900), 311 (9 420), 367 (11 100), 648 (155).

Bis{(cyclooctyl)[(2-oxo-1*H*-benzo-1-ylidene)methyl]aminato}-copper(II) 3. Yield 0.41 g, 79%; brown crystals; m.p. 169 °C. Found C, 68.7; H, 9.0; N, 6.3; calc. for $C_{30}H_{40}N_2O_2Cu$: C, 68.8; H, 9.1; N, 6.2%. FAB-MS *m*/*z*: M^+ 524 (base peak). IR (KBr): ν (C=N) 1616 cm^{-1}. μ_{eff} 1.93 B.M. UV/vis ($CHCl_3$) λ/nm (ε/M^{-1} cm^{-1}): 248 (39 000), 312 (9610), 366 (11550), 630 (160).

Bis{(cyclopentyl)[(2-oxo-1*H*-naphth-1-ylidene)methyl]-aminato}copper(II) 4. Yield 0.43 g, 80%; brown crystals; m.p. 238 °C. Found C, 71.2; H, 6.0; N, 5.2; calc. for $C_{32}H_{32}N_2O_2Cu$: C, 71.1; H, 6.0; N, 5.2%. FAB-MS *m*/*z* M^+ 540 (base peak 154). IR (KBr): ν (C=N) 1609 cm^{-1}. μ_{eff} 1.87 B.M. UV/vis ($CHCl_3$) λ/nm (ε/M^{-1} cm^{-1}): 252 (53 320), 316 (31 870), 383 (12 425), 397 (12 325).

Bis{(cycloheptyl)[(2-oxo-1*H*-naphth-1-ylidene)methyl]-aminato}copper(II) 5. Yield 0.48 g, 81%; brown crystals; m.p. 216–218 °C. Found C, 72.5; H, 6.8; N, 4.7; calc. for $C_{36}H_{40}N_2O_2Cu$: C, 72.6; H, 6.8; N, 4.8%. FAB-MS *m*/*z* M^+ 596 (base peak 154). IR (KBr): ν (C=N) 1610 cm^{-1}. μ_{eff} 1.83 B.M. UV/vis ($CHCl_3$) λ/nm (ε/M^{-1} cm^{-1}): 251 (53 770), 316 (32 320), 382 (12 760), 395 (12 480).

Bis{(cyclooctyl)[(2-oxo-1*H*-naphth-1-ylidene)methyl]-aminato}copper(II) 6. Yield 0.54 g, 87%; brown crystals; m.p. 214–215 °C. Found C, 73.1; H, 7.2; N, 4.6; calc. for $C_{38}H_{44}N_2O_2Cu$: C, 73.0; H, 7.1; N, 4.5%. FAB-MS *m*/*z* M^+ 624 (base peak). IR (KBr): ν (C=N) 1615 cm^{-1}. μ_{eff} 1.87 B.M. UV/vis ($CHCl_3$) λ/nm (ε/M^{-1} cm^{-1}): 251 (57 775), 316 (34 720), 381 (13 800), 395 (13 415).

Electrochemistry

Cyclic voltammetry and double potential step experiments were carried out by using a conventional three-electrode cell, having a platinum disc electrode with an area of 3.14 mm^2 as the working electrode which, prior to the measurements, was cleaned

and polished with 0.05 micron alumina (Buehler Ltd.), wiped with a tissue, washed with distilled water and finally, with acetone. The counter electrode consisted of a piece of platinum wire. The reference electrode, to which all potentials are referred was an aqueous saturated calomel electrode (SCE) isolated from the main cell by a Luggin tube filled with solvent and supporting electrolyte. Solutions in the Luggin tube were changed periodically to prevent aqueous contamination from entering the cell from the SCE. Test solutions containing 1 mM of copper(II) complex and 0.1 M of Et_4NBF_4 in DMF were deoxygenated for 15 min. with nitrogen saturated with solvent vapour. All measurements were carried out at room temperature. The electroactivity range for this system was 3.6 V (from 1.6 to −2.0 V *vs.* SCE).

Cyclic voltammetry[14] and chronocoulometry[12] were carried out using a Bioanalytical Systems BAS 100 B/W electrochemical analyzer interfaced with a Gateway 2000 personal computer. Cyclic voltammograms were measured with variable sweep rates from 0.01 to 10 V s^{-1} and the *i*R drop was compensated for. For chronocoulometry experiments, a mean of three determinations was made for each width pulse which was applied from 10 to 100 ms.

EPR

The EPR measurements were performed on a JEOL JES TE300 spectrometer. A nitrogen based JEOL DVT cryogenic attachment was used. An external JEOL ES-FC5 NMR precision field-meter was used for calibration of the magnetic field. All compounds show EPR response in a 1×10^{-2} M DMF solution at 193 K for the Cu–2,3-*N*-cycloalkyl compounds and 203 K for the Cu–sal-*N*-cycloalkyl and Cu–1,2-*N*-cycloalkyl sequences.

X-Ray crystallography

Suitable X-ray quality crystals of complexes **1**–**5** were grown by slow layer diffusion of MeOH into saturated CH_2Cl_2 solutions, while crystals of **6** were obtained from a (1 : 1) mixture of MeCN–CH_2Cl_2. Data were collected on a Siemens P4/PC diffractometer using Mo-Kα radiation ($\lambda = 0.7173$ Å) with a graphite-monochromator. Structures were solved by direct methods using the SHELXS-97[20] program. In the final cycles of refinement, all non-hydrogen atoms were refined with anisotropic thermal parameters, except for compounds **3** and **6**, in which the eight-membered rings showed disordered thermal motion ellipsoids and were modeled in two positions by using constraints and restraints on the occupational thermal positions and C–C bond distances using SHELXL-97.[21] Neutral atomic scattering factors were taken from the *International Tables for X-Ray Crystallography*.[22]

CCDC reference numbers 154192–154197.

See http://www.rsc.org/suppdata/dt/b1/b104892a/ for crystallographic data in CIF or other electronic format.

Acknowledgements

We thank Dr Paul R. Raithby for helpful suggestions. We are grateful to Consejo Nacional de Ciencia y Tecnología (CONACyT) for the financial support given *via* grant no. 28016E and for a fellowship to N. M.-R. N. M.-R. is also indebted to DGEP-UNAM for a complementary fellowship. M. A.-M. is on leave from Departamento de Fisicoquímica, División de Estudios de Posgrado, Facultad de Química, U.N.A.M. Circuito Escolar, Ciudad, Universitaria, Coyoacán 04510, México, D.F. México.

References

1 G. S. Patterson and R. H. Holm, *Bioinorg. Chem.*, 1975, **4**, 257.
2 P. Zanello, *Stereochemistry of Organometallic and Inorganic Compounds*, ed. I. Bernal, Elsevier, Amsterdam, 1991, vol. 4, p. 180.
3 R. H. Holm and M. J. O'Connor, *Prog. Inorg. Chem.*, 1971, **14**, 241.
4 H. S. Maslen and T. N. Waters, *Coord. Chem. Rev.*, 1975, **17**, 137.
5 G. V. Panova, N. K. Vikulova and V. M. Potapov, *Russ. Chem. Rev.*, 1980, **49**, 655.
6 (*a*) J. M. Fernández-G., S. Hernández-Ortega, R. Cetina-Rosado, N. Macías-Ruvalcaba and M. Aguilar-Martínez, *Polyhedron*, 1998, **17**, 2425; (*b*) J. M. Fernández-G., M. R. Patiño-Maya, R. A. Toscano, L. Velasco, M. Otero-López and M. Aguilar-Martínez, *Polyhedron*, 1997, **16**, 4371.
7 M. Takayama, Y. Tanaka and T. Nomura, *Org. Mass Spectrom.*, 1993, **28**, 1529.
8 L. Sacconi and M. Ciampolini, *J. Chem. Soc.*, 1964, 276.
9 J. E. Kovacic, *Spectrochim. Acta, Part A*, 1967, **23**, 183.
10 H. Tamura, K. Ogawa, A. Takeuchi and S. Yamada, *Chem. Lett.*, 1977, 889.
11 T. P. Cheesman, D. Hall and T. N. Waters, *J. Chem. Soc. A*, 1966, 685.
12 A. J. Bard and L. R. Faulkner, *Electrochemical Methods Fundamentals and Applications*, John Wiley & Sons, New York, 1980.
13 W. E. Geiger, *Prog. Inorg. Chem.*, 1985, **33**, 275.
14 R. S. Nicholson, *Anal. Chem.*, 1966, **37**, 1351.
15 J. A. Mac Phee, A. Panaye and J. E. Dubois, *Tetrahedron*, 1978, **34**, 3555.
16 J. M. Fernández-G., M. J. Rosales-Hoz, M. F. Rubio-Arroyo, R. Salcedo, R. A. Toscano and A. Vela, *Inorg. Chem.*, 1987, **26**, 349.
17 J. R. Wasson, H. W. Richardson and W. E. Hatfield, *Z. Naturforsch., Teil B*, 1977, **32**, 551.
18 F. Vögtle, *Supramolecular Chemistry*, John Wiley & Sons, New York, 1993.
19 G. L. Eichhorn and M. D. Marchand, *J. Am. Chem. Soc.*, 1956, **78**, 2688.
20 G. M. Sheldrick, SHELXS-97, v. 97-1, Crystal Structure Solution, Institut Anorg. Chemie, Universität Göttingen, Germany, 1997.
21 G. M. Sheldrick SHELXL-97, v. 97-1, Crystal Structure Refinement, Institut Anorg. Chemie, Universität Göttingen, Germany, 1997.
22 D. T. Cromer and J. T. Waber, *International Tables for X-Ray Crystallography*, The Kynoch Press, Birmingham, 1974, vol. 4.